

Information-Geometric Signatures from Nonextensivity in the 1-D Blume-Capel Model

Amijit Bhattacharjee^{1,*}, Himanshu Bora^{2,†} and Prabwal Phukon^{1,3‡}

1. Department of Physics, Dibrugarh University, Dibrugarh, Assam, 786004.

2. Department of Physics, Kamrup College, Chamata, Nalbari, Assam - 783006, India

*3. Theoretical Physics Division, Centre for Atmospheric Studies,
Dibrugarh University, Dibrugarh, Assam, 786004.*

We study the thermodynamic geometry of the one-dimensional Blume–Capel model within the Tsallis nonextensive framework to understand how generalized statistics modify correlation structure and pseudo-critical behaviour. Using the transfer matrix method, we construct the Tsallis entropy based thermodynamic metric as its negative Hessian on the parameter space (β, J) , with the crystal-field anisotropy D as a control parameter, and compute the associated scalar curvature $R(T)$ as a measure of correlations. Although no true phase transition occurs in one dimension, $R(T)$ exhibits finite peaks signaling pseudo-critical crossovers. We analyze both $D < J$ and $D > J$ regimes and show that deviations from the Boltzmann–Gibbs limit ($q = 1$) systematically deform the curvature profile: for $q > 1$ the peak shifts and correlations persist beyond the crossover, whereas for $q < 1$ the peak is weakened or suppressed. Our results demonstrate that the Tsallis parameter q geometrically reshapes the entropy surface, providing a clear information-geometric interpretation of nonextensive effects in spin-1 systems.

I. INTRODUCTION

The thermodynamic geometric approach provides a profound and unified framework for describing equilibrium thermodynamics through Riemannian structures defined on the manifold of thermodynamic states. Originally introduced by Frank Weinhold [1] and further developed by George Ruppeiner [2, 3], this formalism associates a metric tensor to the space of equilibrium parameters, with the scalar curvature R encoding information about the underlying microscopic correlations. In this geometric picture, a vanishing curvature corresponds to non-interacting systems, while large or divergent curvature signals strong correlations and critical behaviour. Over the years, thermodynamic geometry has emerged as a powerful diagnostic tool in diverse contexts, including magnetic systems [4], quantum gases [5], black holes [6–8], and condensed matter models [9–11].

Among lattice spin systems, the Blume–Capel (BC) model [12–14] occupies a distinguished position as a natural generalization of the Ising model. Unlike the spin- $\frac{1}{2}$ Ising system, the Blume–Capel model incorporates an additional spin state $S_i = 0$, representing a non-magnetic or vacancy configuration, alongside the magnetic states $S_i = \pm 1$. The presence of the single-ion anisotropy parameter D introduces a competition between magnetic ordering and vacancy formation, enriching the thermodynamic structure of the model. In higher dimensions, this competition gives rise to tricritical behavior and first-order phase transitions, making the Blume–Capel model a prototypical system for studying multicritical phenomena.

Even in one dimension, where no true thermodynamic phase transition occurs at finite temperature, the model exhibits sharp crossovers and pseudo-critical behaviour for specific ranges of the ratio D/J . These features manifest through pronounced variations in response functions and correlation lengths. From a geometric standpoint, such pseudo-critical effects are reflected in peaks of the thermodynamic scalar curvature $R(T)$, which measures the effective correlation volume. The analytical tractability of the one-dimensional case via the transfer matrix method makes it an ideal laboratory for exploring how modifications in statistical structure influence thermodynamic geometry.

Beyond the conventional Boltzmann–Gibbs framework, generalized entropy formalisms have attracted considerable attention in the study of complex systems characterized by long-range interactions, fractal phase-space structures, or memory effects. In particular, the entropy proposed by Tsallis introduces a deformation parameter q that controls deviations from extensivity. For $q \rightarrow 1$, the standard Boltzmann–Gibbs entropy is recovered, whereas for $q \neq 1$, the statistical weights of microstates are modified, effectively enhancing or suppressing rare configurations depending on the direction of deviation. Such nonextensive frameworks have been successfully applied to gravitational clustering,

* *rs_amijitbhattacharjee@dibru.ac.in*

† *hb@kamrupcollege.ac.in*

‡ *prabwal@dibru.ac.in*

turbulence, anomalous diffusion, and strongly correlated systems. A brief summary of the Tsallis entropy is as follows:

Tsallis Entropy: Put forward by Constantino Tsallis in 1988, Tsallis entropy [15–21] is a generalization of the Boltzmann-Gibbs entropy that aims to describe systems exhibiting long-range interactions, memory effects, or multifractal structures with conditions under which the standard additive entropy fails. It is defined as

$$S_q = \frac{1 - \sum_i p_i^q}{q - 1},$$

where q is the entropic index that measures the degree of non-extensivity. For $q \rightarrow 1$, Tsallis entropy recovers the usual Boltzmann-Gibbs form. When $q > 1$, rare events (low-probability states) are suppressed, while for $q < 1$, they are enhanced, allowing the entropy to model diverse physical systems such as turbulent flows, gravitational clustering, and anomalous diffusion. Its non additive property makes it particularly suitable for complex systems where correlations between subsystems are significant.

Here the exponent q modifies the sensitivity of the entropy to various probability values. When $q > 1$, higher probabilities are effectively emphasized because raising $p_i \leq 1$ to a power greater than one suppresses smaller probabilities more strongly than larger ones. Consequently, rare events contribute less, and the entropy becomes more sensitive to dominant (main) events. In contrast, when $q < 1$, small probabilities are relatively enhanced since p_i^q with $q < 1$ increases the weight of rare events compared to the standard case. As a result, the entropy becomes more sensitive to the tails of the distribution, favouring fluctuations and uncommon configurations. In the limit $q \rightarrow 1$, one recovers the usual Boltzmann-Gibbs entropy as the follows:

The Tsallis entropy is given as:

$$S_q = \frac{1 - \sum_i p_i^q}{q - 1}. \quad (1)$$

We rewrite

$$\sum_i p_i^q = \sum_i p_i e^{(q-1) \ln p_i}. \quad (2)$$

For $q \rightarrow 1$, we have

$$(q - 1) \ll 1.$$

Therefore, using the Taylor expansion,

$$e^{(q-1) \ln p_i} = 1 + (q - 1) \ln p_i. \quad (3)$$

Substituting the eqtn. 2 into eqtn.1, we get

$$\sum_i p_i^q = \sum_i p_i (1 + (q - 1) \ln p_i) \quad (4)$$

$$= \sum_i p_i + (q - 1) \sum_i p_i \ln p_i. \quad (5)$$

Therefore,

$$S_q = \frac{1 - \sum_i (p_i + (q - 1)p_i \ln p_i)}{q - 1}. \quad (6)$$

Since $\sum_i p_i = 1$, we obtain

$$S_q = \frac{1 - 1 - (q - 1) \sum_i p_i \ln p_i}{q - 1} \quad (7)$$

$$= - \sum_i p_i \ln p_i. \quad (8)$$

Hence,

$$\lim_{q \rightarrow 1} S_q = S_{BG} = - \sum_i p_i \ln p_i. \quad (9)$$

Therefore in the limit $q \rightarrow 1$, the Tsallis entropy S_q reduces to the usual Boltzmann-Gibbs entropy as follows:

$$S = S_{BG} = - \sum_i p_i \ln p_i,$$

When generalized entropies are employed, thermodynamic potentials and response functions acquire modified functional forms, and consequently the geometry of the entropy surface is altered. Since the thermodynamic metric is defined as the negative Hessian of the entropy with respect to its parameters, any deformation of the entropy directly reshapes the underlying geometric manifold. The scalar curvature therefore serves as a sensitive probe of how nonextensivity modifies correlation strength, stability properties, and pseudo-critical structure.

In the present work, we investigate the one-dimensional Blume–Capel model within the Tsallis nonextensive framework using an entropy-based thermodynamic metric defined on the parameter space (β, J) , with the crystal field D acting as a control parameter. By constructing the metric tensor

$$g_{ij} = -\partial_i \partial_j S_q(\beta, J),$$

and computing the associated scalar curvature $R(T)$, we analyze how the deformation parameter q modifies the curvature–temperature profile and the location and magnitude of pseudo-critical peaks. Our goal is to provide a geometric interpretation of nonextensive effects in spin-1 systems and to clarify how the interplay between exchange interaction and single-ion anisotropy is reshaped under generalized statistics.

The remainder of the paper is organized as follows. In Section II, we present the 1D Blume-Capel model and transform it with the Tsallis entropy framework. Section III develops the metric structure and thus its Tsallis generalization. Section IV is devoted to the thermodynamic geometric analysis of the non-extensive 1D Blume-Capel model. We provide a discussion on the obtained results in Section V. We conclude with a short summary in Section VI.

II. THE ONE-DIMENSIONAL BLUME CAPEL MODEL

The *Theory of the First-Order Magnetic Phase Change in UO_2* [12] by Melvin Blume marked the conceptual birth of what later came to be known as the Blume-Capel model. It arose from the need to explain the experimentally observed first-order anti-ferromagnetic transition in UO_2 , which could not be satisfactorily accounted for by conventional Heisenberg models containing only bilinear exchange interactions. Blume proposed a simple yet profound mechanism: the uranium ion possesses a non-magnetic singlet ground state and a low-lying magnetic triplet split by crystal-field effects, and the exchange interaction treated within a molecular-field approximation, can self-consistently drive a crossing between these levels. As the temperature increases, thermal population of the non-magnetic singlet reduces the exchange splitting, potentially causing a discontinuous collapse of magnetization, *i.e.*, a first-order phase transition. Abstracting from the specific ionic structure of UO_2 , this physical picture was later reformulated in terms of spin-1 variables with three possible states $(-1, 0, +1)$, where the crystal-field splitting acts as a single-ion anisotropy term that energetically favours or disfavors the $S = 0$ state. The resulting minimal Hamiltonian consisting of bilinear exchange together with a crystal-field term became the Blume-Capel model, providing a unified framework for the study of tri-criticality, first and second-order phase transitions, and vacancy-like spin states in magnetic systems.

As is described above, the Blume–Capel (BC) model is a spin-1 generalization of the Ising model, originally introduced to describe systems with both magnetic and non-magnetic states. Each spin variable S_i can take three possible values,

$$S_i \in \{-1, 0, +1\},$$

where the state $S_i = 0$ represents a vacancy or a non-magnetic configuration. The Blume-Capel model, originally put forward independently by Blume [12] and Capel [13], has become an important and a foundational framework for studying tri-critical behaviour [22–29]. One of its strikingly distinguishing features is its capacity to model transitions from second-order to first-order phase transitions and thereby revealing intricate critical behaviours. The model has been investigated using diverse approaches which includes the mean-field theory [12, 13], renormalization group techniques [30], and Monte Carlo simulations [31–33]. Research on the Blume-Capel model has covered a wide range of materials which includes metallic alloys [34–37], magnetic thin films [38], and superconducting thin films [25]. In addition to its applications in physics, the model has been extensively employed in sociology, particularly in recent studies on depolarization [39, 40]. Owing to the fact that its critical importance and capacity to capture a wide range of phase behaviours the Blume-Capel model has generated a wide range of publications [41–44].

II.1. Hamiltonian without External Magnetic Field

In the absence of an external magnetic field, the Hamiltonian of the Blume–Capel model is given by [14]

$$\mathcal{H} = -J \sum_{\langle i,j \rangle} S_i S_j + D \sum_i S_i^2,$$

where:

- J is the nearest-neighbor exchange interaction strength,
- D is the single-ion crystal field anisotropy,
- $\langle i,j \rangle$ denotes a sum over nearest-neighbor pairs.

The first term favors ferromagnetic alignment for $J > 0$, while the second term controls the population of the $S_i = 0$ state. For large positive D , the non-magnetic state is energetically favored, whereas for large J , the magnetic states $S_i = \pm 1$ dominate.

II.2. Transfer Matrix Formulation

For a one-dimensional lattice with periodic boundary conditions, the partition function can be computed exactly using the transfer matrix method. The partition function is

$$Z = \sum_{\{S_i\}} \exp \left[\beta J \sum_i S_i S_{i+1} - \beta D \sum_i S_i^2 \right],$$

where $\beta = 1/(k_B T)$. The transfer matrix \mathbf{T} is defined by

$$\mathbf{T}_{S,S'} = \exp \left[\beta J S S' - \frac{\beta D}{2} (S^2 + S'^2) \right],$$

with $S, S' \in \{-1, 0, +1\}$. Explicitly, in the basis $\{+1, 0, -1\}$, the transfer matrix takes the form

$$\mathbf{T} = \begin{pmatrix} e^{\beta J - \beta D} & e^{-\beta D/2} & e^{-\beta J - \beta D} \\ e^{-\beta D/2} & 1 & e^{-\beta D/2} \\ e^{-\beta J - \beta D} & e^{-\beta D/2} & e^{\beta J - \beta D} \end{pmatrix}.$$

The partition function for a chain of N spins is then

$$Z = \text{Tr } \mathbf{T}^N,$$

$$Z(\beta, J, D) = E_1(\beta, J, D)^N + E_2(\beta, J, D)^N + E_3(\beta, J, D)^N$$

where $E_1(\beta, J, D)$, $E_2(\beta, J, D)$ and $E_3(\beta, J, D)$ are the eigenvalues of the transfer matrix T . They are given as

$$E_1(\beta, J, D) = 2e^{-\beta D} \sinh(\beta J)$$

$$E_2(\beta, J, D) = \frac{1}{2} \left[1 + 2e^{-\beta D} \cosh(\beta J) + \sqrt{(1 + 2e^{-\beta D} \cosh(\beta J))^2 - 8e^{-\beta D}} \right]$$

$$E_3(\beta, J, D) = \frac{1}{2} \left[1 + 2e^{-\beta D} \cosh(\beta J) - \sqrt{(1 + 2e^{-\beta D} \cosh(\beta J))^2 - 8e^{-\beta D}} \right]$$

To isolate the extensive bulk behavior from finite-size effects, we must factor out the strictly dominant eigenvalue. As we shall later see, this also helps in computational stability of the numerical calculations. We can argue that

E_2 is always the largest eigenvalue for any physical parameter set ($\beta(T), J, D$ being real and finite) invoking the Perron-Frobenius Theorem, which states that for any matrix with strictly positive entries, there is a unique largest eigenvalue and its corresponding eigenvector is the only one whose components can be chosen to be all strictly positive.

The transfer matrix T consists entirely of strictly positive exponential terms ($T_{ij} > 0$ for all physical parameters). The eigenvalue E_1 corresponds to the antisymmetric eigenvector $(1, 0, -1)^T$ and since this eigenvector contains a negative component, so E_1 can not be the dominant eigenvalue. We are therefore left with the roots E_2 and E_3 from the symmetric subspace. E_2 is formed by adding the strictly positive principal square root of the discriminant, and hence $E_2 > E_3$ is unconditionally true. Therefore, E_2 must be the unique dominant eigenvalue.

Factoring out the dominant eigenvalue E_2 , the partition function is rewritten as:

$$Z(\beta, J, D) = E_2(\beta)^N \left(1 + \left(\frac{E_1(\beta)}{E_2(\beta)} \right)^N + \left(\frac{E_3(\beta)}{E_2(\beta)} \right)^N \right) = E_2(\beta)^N (1 + \Omega_N(\beta)) \quad (10)$$

where $\Omega_N(\beta) = (E_1/E_2)^N + (E_3/E_2)^N$ acts as the finite-size correction term. As $N \rightarrow \infty$, the term $\Omega_N \rightarrow 0$ exponentially.

The Tsallis entropy is defined as:

$$S_q = \frac{1 - \sum_i p_i^q}{q - 1}, \quad (11)$$

which can be rewritten in terms of the partition function using the canonical probabilities,

$$S_q = \frac{1}{q - 1} \left(1 - \frac{Z(q\beta)}{Z(\beta)^q} \right) \quad (12)$$

Defining the bulk deformation potential $\Delta_q \equiv q \ln E_2(\beta) - \ln E_2(q\beta)$, we substitute the factored partition function to obtain a numerically stable formulation:

$$S_q = \underbrace{\frac{1 - e^{-N\Delta_q}}{q - 1}}_{S_{\text{bulk}}} + \underbrace{\frac{e^{-N\Delta_q}}{q - 1} \left[1 - \frac{1 + \Omega_N(q\beta)}{(1 + \Omega_N(\beta))^q} \right]}_{S_{\text{corr}}} \quad (13)$$

To illustrate the suppression of the finite-size corrections as N increases, Figure 1 demonstrates the decay of the correlation ratio Ω_N and S_{corr} .

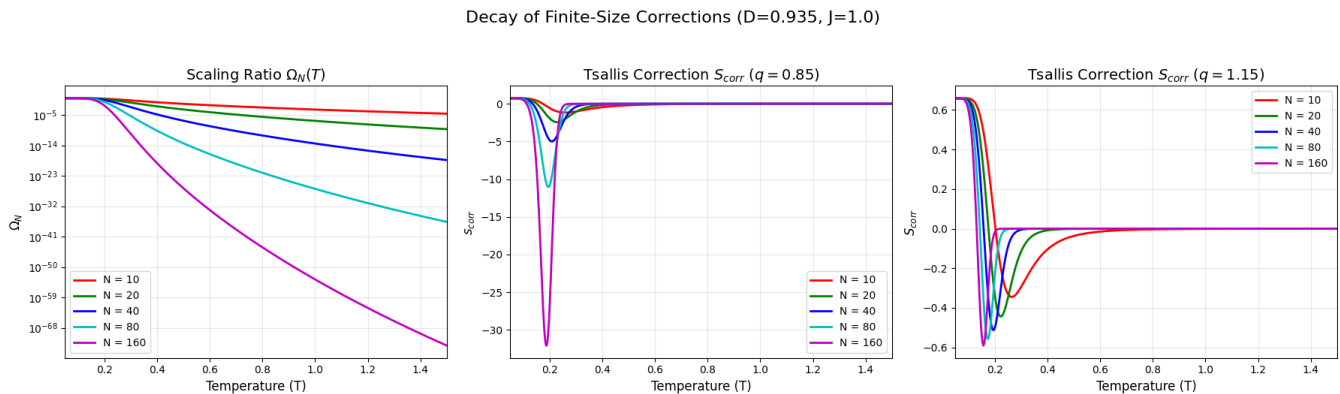


FIG. 1: (left) Scaling of the finite-size correction term Ω_N as a function of temperature for various system sizes N and decay of S_{corr} in $q < 1$ (centre) and $q > 1$ (right) regimes as a function of temperature for various system sizes N . As N increases, the finite-size correction term Ω_N vanishes rapidly and S_{corr} approaches 0, isolating the bulk geometry.

II.3. Remarks

Although the one-dimensional Blume-Capel model does not exhibit a true phase transition at finite temperature, it shows sharp crossovers or pseudo-critical behaviour for certain values of D/J . These features become particularly relevant when generalized entropy formalisms, such as Tsallis entropy, is employed, where effective long-range correlations can emerge even in low-dimensional systems.

III. THERMODYNAMIC METRIC AND GEOMETRIC STRUCTURE

III.1. Motivation and Conceptual Basis

Thermodynamic geometry offers a powerful formalism that connects macroscopic thermodynamic behavior with the differential geometry of the entropy or energy surfaces. The idea originated from the works of Weinhold[1] and Ruppeiner [2, 3], who independently proposed Riemannian metrics on the thermodynamic state space. In this approach, the equilibrium manifold is endowed with a metric whose curvature encodes the strength and nature of thermodynamic correlations among microscopic degrees of freedom. The scalar curvature R derived from this metric provides a geometric interpretation of phase transitions, criticality, and statistical interactions. For instance, $R = 0$ corresponds to an ideal gas where microstates are uncorrelated, while a diverging R signifies critical behavior where correlation length diverges [4, 45, 46].

The construction of the thermodynamic metric is grounded in fluctuation theory. Consider the probability distribution of fluctuations around equilibrium in an ensemble characterized by extensive variables X^i and their conjugate intensive variables Y_i . In the Gaussian approximation, the probability of a fluctuation dX^i away from equilibrium is given by

$$P \propto \exp\left(-\frac{1}{2}g_{ij} dX^i dX^j\right), \quad (14)$$

where g_{ij} acts as the inverse covariance matrix of the fluctuations and hence defines the thermodynamic metric tensor. For the entropy representation, the line element is defined as

$$ds^2 = -\frac{\partial^2 S}{\partial X^i \partial X^j} dX^i dX^j, \quad (15)$$

which ensures that the entropy is maximized at equilibrium, implying that the metric is positive definite. This formulation is equivalent to defining the metric as the Hessian of the Massieu potential, linking it directly to the second derivatives of the entropy with respect to its natural variables. Weinhold's earlier definition, in contrast, was based on the internal energy representation,

$$g_{ij}^{(W)} = \frac{\partial^2 U}{\partial X^i \partial X^j}, \quad (16)$$

and it can be shown that the Ruppeiner and Weinhold metrics are conformally related by the temperature:

$$g_{ij}^{(R)} = \frac{1}{T} g_{ij}^{(W)}. \quad (17)$$

This relation underscores that both metrics convey the same geometric information but differ in their thermodynamic potentials.

III.2. Geometric Interpretation of the Scalar Curvature

Using the generalized entropy function $S(\beta, J)$ corresponding to either Rényi or Tsallis forms, the entropy-based thermodynamic metric on the parameter manifold (β, J) is defined as

$$g_{ij} = -\frac{\partial^2 S(\beta, J)}{\partial x^i \partial x^j}, \quad x^i = (\beta, J). \quad (18)$$

The associated Ricci scalar curvature $R(\beta, J)$ is computed from the metric tensor, and its temperature dependence $R(T)$ provides a geometric measure of thermodynamic correlations. In the nonextensive regime, deviations in $R(T)$

relative to the Boltzmann–Gibbs case reflect how the generalized entropy modifies the effective correlation volume and pseudo-critical structure of the spin chain.

In non-extensive statistical mechanics, the entropy no longer scales additively with subsystem size due to the presence of long-range correlations or fractal phase-space structures. Consequently, the fluctuation geometry must be adapted to incorporate the deformation introduced by generalized entropies such as those of Rényi and Tsallis. The underlying principle remains the same: the metric measures the local curvature of the entropy surface in the space of control parameters, reflecting how stable the equilibrium state is under small perturbations.

Given a generalized entropy $S(\beta, J)$, depending on intensive variables such as the inverse temperature β and coupling constant J , we define the metric as

$$g_{ij} = -\frac{\partial^2 S(\beta, J)}{\partial x^i \partial x^j}, \quad x^i = (\beta, J), \quad (19)$$

where the negative sign ensures positive definiteness of the metric because entropy is a concave function of its natural variables. This formulation departs from the traditional extensive representation where the coordinates are extensive variables like U , V , or N . Instead, it constructs an *entropy-based metric on the parameter manifold*, an approach that is particularly useful for systems such as spin chains or black holes, where β and J are more natural variables than energy or volume [47, 48].

The physical meaning of the components of this metric can be interpreted as follows:

$$\begin{aligned} g_{\beta\beta} &= -\frac{\partial^2 S}{\partial \beta^2} \Rightarrow \text{fluctuations in temperature,} \\ g_{\beta J} &= -\frac{\partial^2 S}{\partial \beta \partial J} \Rightarrow \text{cross-correlation between temperature and coupling,} \\ g_{JJ} &= -\frac{\partial^2 S}{\partial J^2} \Rightarrow \text{fluctuations in the interaction strength.} \end{aligned} \quad (20)$$

The determinant of the metric $\det(g_{ij})$ quantifies the joint stability of the system with respect to simultaneous changes in β and J , and its inverse defines the volume element in parameter space associated with thermodynamic fluctuations.

Once the metric tensor g_{ij} is defined, the Riemann curvature tensor and the scalar curvature R can be computed using standard differential-geometric formulae. To determine the thermodynamic scalar curvature for a given thermodynamic metric, one follows the standard procedure of Riemannian geometry, with the metric defined on the space of equilibrium states. Let the metric be denoted by $g_{ij}(X^k)$, where X^k represent the thermodynamic coordinates (such as entropy, charge, angular momentum, etc.). The first step is to compute the inverse metric g^{ij} . One then evaluates the Christoffel symbols accordingly as:

$$\Gamma^i_{jk} = \frac{1}{2} g^{il} (\partial_j g_{lk} + \partial_k g_{lj} - \partial_l g_{jk}).$$

Using these, the Riemann curvature tensor is constructed by the given formula:

$$R^i_{jkl} = \partial_k \Gamma^i_{jl} - \partial_l \Gamma^i_{jk} + \Gamma^i_{km} \Gamma^m_{jl} - \Gamma^i_{lm} \Gamma^m_{jk}.$$

Contracting indices gives the Ricci tensor,

$$R_{jl} = R^i_{jil},$$

and finally the thermodynamic scalar curvature is obtained by a further contraction with the inverse metric,

$$R = g^{jl} R_{jl}.$$

The resulting scalar R encodes information about thermodynamic interactions and phase transitions; in many systems, divergences of R are associated with critical points, while its sign is often interpreted as reflecting the nature of the underlying microscopic interactions. The scalar curvature acts as a geometric diagnostic of interactions: $R > 0$ typically indicates dominant repulsive correlations, $R < 0$ suggests attractive correlations, and $|R|$ is proportional to the correlation volume ξ^d , with ξ being the correlation length and d the dimensionality of the system [4, 46]. Investigating the thermodynamic geometry of the one-dimensional Blume-Capel model by calculating the thermodynamic curvature scalar R , we must perform numerical calculations. Exact analytical computations of the scalar curvature

become excruciatingly complex due to the highly nonlinear nature of the generalized entropy and the requirement for high-order derivatives. To overcome this, we perform numerical calculations using **JAX**, a high-performance numerical computing python library that provides composable transformations, notably exact Automatic Differentiation (**AutoDiff**) and Just-In-Time (**JIT**) compilation. We do not use finite-difference methods since they are highly susceptible to truncation and floating-point rounding errors. When computing higher-order derivatives, **AutoDiff** evaluates derivatives analytically at the graph level.

While the standard differential-geometric procedure for calculating the scalar curvature R involves computing the inverse metric, the Christoffel symbols Γ_{jk}^i , the Riemann curvature tensor, and subsequent tensor contractions, implementing this step-by-step tensor algebra numerically is computationally inefficient. For a two-dimensional thermodynamic manifold with the metric tensor components defined as $E = g_{\beta\beta}$, $F = g_{\beta J}$, and $G = g_{JJ}$, we can bypass the intermediate Christoffel symbols by utilizing the algebraically equivalent Brioschi formula. This approach is mathematically identical to the Christoffel symbol contraction but is vastly superior for vectorized automatic differentiation, as it compiles into a single, highly optimized computational graph. Calculating the Ricci scalar R via the Brioschi formula requires the second derivatives of the metric components, which ultimately correspond to the fourth-order derivatives of the generalized entropy with respect to the thermodynamic parameters (β, J) . To ensure numerical stability during these extensive derivative calculations, we resort to enforcing all computational graphs in our code to operate in 64-bit precision as standard 32-bit floating-point precision is insufficient.

We begin the calculation with the exact finite-size formulation of the model as has been derived in eq.13. To ensure continuous differentiability during **AutoDiff**, we employ branch-less programming techniques (such as smooth maximum and minimum functions) to consistently sort the remaining sub-dominant eigenvalues without breaking the computational graph. We implemented the entropy function $S(\beta, J)$ as a unified function capable of evaluating the Tsallis framework utilizing all three eigenvalues. To smoothly handle the Boltzmann-Gibbs limit ($n \rightarrow 1$ or $q \rightarrow 1$), we enforced a safe numerical convergence shift (evaluating at 1.0001) to bypass zero-division errors while preserving the desired asymptotic accuracy.

The computational pipeline for the geometry followed a three-step derivative process using JAX's transformation primitives. We extracted the metric components $E = g_{\beta\beta}$, $F = g_{\beta J}$, and $G = g_{JJ}$ by applying the Hessian operator directly to the entropy scalar function, returning the exact 2×2 covariance matrix at any point (β, J) . Then we applied the forward-mode Jacobian operator to the metric component vector \mathbf{x} , after which, we applied a secondary Hessian operator to the metric components to yield the required higher-order cross-derivatives $(E_{JJ}, G_{\beta\beta}, F_{\beta J})$. Next, we substitute the computed metric components and their derivatives directly into the Brioschi determinant formula. The Brioschi formula directly expresses the Gaussian curvature K entirely in terms of the metric components and their first and second partial derivatives:

$$K = \frac{1}{(EG - F^2)^2} \left(\begin{vmatrix} -\frac{1}{2}E_{JJ} + F_{\beta J} - \frac{1}{2}G_{\beta\beta} & \frac{1}{2}E_{\beta} & F_{\beta} - \frac{1}{2}E_J \\ F_J - \frac{1}{2}G_{\beta} & E & F \\ \frac{1}{2}G_J & F & G \end{vmatrix} - \begin{vmatrix} 0 & \frac{1}{2}E_J & \frac{1}{2}G_{\beta} \\ \frac{1}{2}E_J & E & F \\ \frac{1}{2}G_{\beta} & F & G \end{vmatrix} \right) \quad (21)$$

In this notation, the straight vertical bars denote the determinant of the 3×3 matrices, and the subscripts denote partial derivatives with respect to the thermodynamic coordinates (e.g., $E_{\beta} = \partial E / \partial \beta$ and $F_{\beta J} = \partial^2 F / \partial \beta \partial J$). The determinants of these matrices are efficiently computed using JAX's linear algebra modules. Finally, the thermodynamic Ricci scalar curvature R for the two-dimensional parameter space is simply given by $R = 2K$.

We generate the high-resolution curvature profiles necessary to accurately capture the ultra-narrow pseudo-critical peaks (e.g., evaluating $R(T)$ across 80,000 grid points) by vectorizing the entire Brioschi computational graph. Combined with **JIT** compilation, this allows the algorithm to compile the deep derivative graph into highly optimized machine code, yielding the exact scalar curvature across the entire parameter domain with high precision and computational efficiency.

In the context of the 1D Blume-Capel model, even though there is no genuine phase transition, the scalar curvature exhibits pseudo-critical peaks corresponding to maxima in the correlation length and also shows non zero scalar curvature, R in certain cases for $q > 1$ regime. These peaks serve as geometric analogs of the crossovers observed in susceptibility and heat capacity. When the entropy is generalized via the Tsallis deformation, the geometry of the entropy surface is altered, leading to a modified curvature profile $R(T)$. The shift of the curvature peak and its magnitude thus provide direct insight into how non-extensivity affects correlations, stability, and information content of the system in effect to change in the Tsallis parameter.

III.3. Physical and Informational Significance

The thermodynamic metric also admits a direct interpretation within information geometry [49, 50]. The metric can be viewed as the Fisher information metric of the probability distribution $p_i(\beta, J)$ associated with the system, since

$$g_{ij} = \sum_i p_i \frac{\partial \ln p_i}{\partial x^i} \frac{\partial \ln p_i}{\partial x^j}, \quad (22)$$

which quantifies the statistical distinguishability between neighbouring thermodynamic states parametrized by x^i . In this sense, the curvature R provides an information-theoretic measure of how sensitive the system is to changes in its thermodynamic parameters. For generalized statistics, the deformation parameter such as the q (Tsallis) modify the effective probability measure, thereby rescaling the Fisher information and reshaping the thermodynamic manifold. The resulting curvature captures the interplay between statistical weighting of microstates and macroscopic stability, establishing a deep connection between information theory, thermodynamics, and geometry.

Broadly speaking, the thermodynamic metric constructed from generalized entropy provides a unified geometric language to describe equilibrium fluctuations, correlation structure, and stability properties. When applied to the one-dimensional Blume-Capel model, it reveals how nonextensive deformations influence the geometry of the entropy surface and the corresponding thermodynamic curvature, offering a novel geometric perspective on generalized statistical mechanics.

IV. THERMODYNAMIC GEOMETRIC ANALYSIS OF THE 1-D BLUME-CAPEL MODEL

IV.1. Tsallis entropy modifications

Combining eq.13 with eq.18 we write the thermodynamic metric for the Tsallis modified Blume-Capel model in (β, J) co-ordinates given by:

$$g_{ij} = -\frac{\partial^2 S_q(\beta, J)}{\partial x^i \partial x^j}, \quad x^i = (\beta, J), \quad (23)$$

where, $S_q(\beta, J)$ is given by eqn.13. Starting from the transfer matrix formulation of the model, the partition function was obtained and subsequently used to construct the Tsallis entropy, which depends explicitly on the inverse temperature β and the interaction strength J , with the crystal-field anisotropy parameter D controlling the relative population of the magnetic ($S = \pm 1$) and non-magnetic ($S = 0$) states. The thermodynamic metric was then defined as the negative Hessian of the generalized entropy with respect to the parameters (β, J) , thereby generating a two-dimensional thermodynamic manifold that captures the response of the entropy surface to fluctuations in temperature and interaction strength. From this metric the associated scalar curvature R was calculated using the standard geometric construction of Riemannian thermodynamics. The curvature was evaluated as a function of temperature for different values of the Tsallis parameter q and for two representative regimes of the anisotropy parameter, namely $D < J$ and $D > J$. Since the one-dimensional Blume-Capel model does not possess a true thermodynamic phase transition at finite temperature, the scalar curvature remains finite throughout the temperature range; however, pronounced peaks appear in $R(T)$ which signal regions of enhanced but finite correlations and therefore act as geometric indicators of pseudo-critical crossover behaviour. We then proceed to compute the thermodynamic scalar from the given metric which is a purely straightforward mathematical calculation. The thermodynamic scalar therefore obtained is plotted against inverse β which is the characteristic temperature of the model denoted as T .

In order to analyze the influence of the crystal-field anisotropy on the thermodynamic geometry of the system, the results are presented separately for two representative parameter regimes characterized by the relative magnitude of the anisotropy parameter D and the exchange interaction J . Specifically, we consider the cases $D < J$ ($D = 0.935$, $J = 1$) and $D > J$ ($D = 1.065$, $J = 1$). For each regime, the thermodynamic scalar curvature $R(T)$ is plotted as a function of temperature for two different system sizes, $N = 60$ and $N = 600$, in order to examine possible finite-size effects and the stability of the pseudo-critical features observed in the curvature profile. Since the scalar curvature is known to provide a geometric measure of the effective correlation volume of the system, its temperature dependence allows us to investigate how the underlying spin configurations and their statistical

weights influence the correlation structure of the Blume–Capel chain.

The distinction between the regimes $D < J$ and $D > J$ has a clear physical interpretation in terms of the relative stability of the allowed spin states. When $D < J$, the exchange interaction dominates over the crystal-field anisotropy, and the energetically favorable configurations are the magnetic states $S = \pm 1$, which tend to align due to the ferromagnetic coupling. In this regime the non-magnetic state $S = 0$ is energetically disfavored and therefore occurs with relatively low probability, effectively behaving as a rare fluctuation in the spin configuration. Consequently, the dominant contributions to the thermodynamic properties arise from configurations composed primarily of $S = \pm 1$ spins, while the $S = 0$ states represent rare events that perturb the magnetic ordering. In contrast, when $D > J$, the crystal-field anisotropy becomes the dominant energy scale and favors the non-magnetic configuration $S = 0$. In this situation the lattice tends to be populated predominantly by $S = 0$ states, while the magnetic states $S = \pm 1$ become energetically suppressed and appear only as thermally excited fluctuations. Thus, in this regime the $S = 0$ configuration represents the most probable or “main” event, whereas the magnetic states act as rare excitations that introduce fluctuations into an otherwise non-magnetic background. By examining the curvature behaviour in these two distinct regimes, we can therefore understand how the thermodynamic geometry responds to changes in the dominant microscopic configurations and how the Tsallis non-extensive parameter modifies the statistical weighting of these common and rare events. With this physical interpretation in mind, we proceed to present the scalar curvature plots for the different parameter ranges.

V. RESULTS AND DISCUSSION

In this section, we analyze the temperature dependence of the thermodynamic scalar curvature $R(T)$ for the one-dimensional Blume–Capel model within the Tsallis entropy formalism. The scalar curvature is computed from the thermodynamic metric defined as the negative Hessian of the generalized entropy with respect to the thermodynamic parameters (β, J) . Since the one-dimensional Blume–Capel model does not exhibit a true phase transition at finite temperature, the appearance of peaks in $R(T)$ is interpreted as a signature of pseudo-critical behaviour associated with enhanced but finite correlation lengths.

The analysis is divided into two regimes depending on the relative strength of the crystal field anisotropy D and the exchange interaction J , namely $D < J$ and $D > J$. For each regime, we examine the behavior of the scalar curvature in the Boltzmann–Gibbs (BG) limit ($q = 1$) and its deformation under the Tsallis entropy for $q > 1$ and $q < 1$. Finite-size effects are studied by comparing system sizes $N = 60$ and $N = 600$.

V.1. $D < J$: Magnetically Dominated Regime

When the exchange interaction dominates over the crystal field anisotropy ($D < J$), the magnetic states $S = \pm 1$ constitute the most probable configurations, while the non-magnetic state $S = 0$ corresponds to a rare event. As we see from Fig. 2 and Fig. 3:

In the Boltzmann–Gibbs limit ($q = 1$), the scalar curvature exhibits a pronounced negative peak around $T \approx 0.24$. The negative sign of R indicates the dominance of attractive correlations associated with short-range ferromagnetic ordering. As the temperature increases beyond this crossover region, the curvature approaches zero, signaling the gradual loss of correlations and the emergence of a paramagnetic phase. This behavior is consistent with the absence of true criticality in one dimension.

For $q > 1$, where rare events are suppressed within the Tsallis framework, the contribution of the $S = 0$ state is reduced. As a result, magnetic correlations are effectively reinforced. This is reflected in a shift of the curvature peak toward lower temperatures while maintaining its negative sign. Moreover, unlike the Boltzmann–Gibbs case, the scalar curvature remains nonzero even beyond the pseudo-transition temperature, indicating the persistence of residual correlations induced by the nonextensive deformation.

In contrast, for $q < 1$, rare events are enhanced, leading to an increased population of the $S = 0$ state. This enhancement disrupts magnetic clustering and weakens ferromagnetic correlations. Consequently, the curvature peak becomes positive and shifts toward higher temperatures, indicating the emergence of repulsion-like or exclusion-dominated correlations. Furthermore, the scalar curvature rapidly approaches zero beyond the crossover region,

suggesting a more efficient suppression of correlations when rare states are amplified.

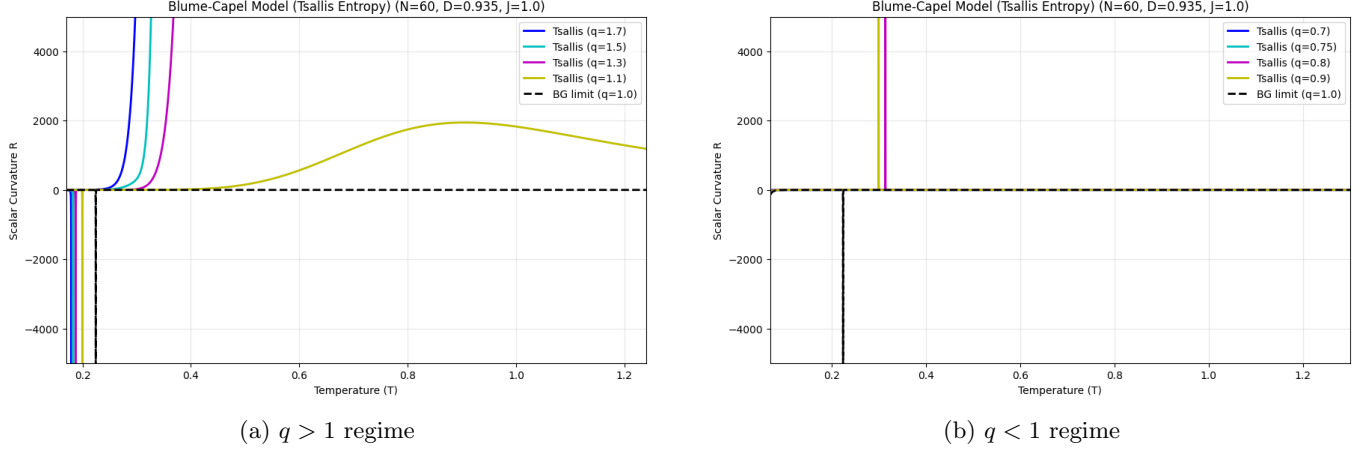


FIG. 2: Temperature dependence of the thermodynamic scalar curvature $R(T)$ for the one-dimensional Blume Capel model using the Tsallis entropy for $(\mathbf{D} < \mathbf{J})$ $D = 0.935$, $J = 1$ and $N = 60$. **(a) For the $q > 1$ regime**, the scalar curvature for the Boltzmann -Gibbs entropy (BG limit) ($q = 1$) lies around $T = 0.24$ and is negative, but for $q > 1$ the curvature peak though still negative shifts towards lower temperatures and the scalar curvature is non zero after the transition takes place for $q > 1$ case whereas it was zero in the previous BG limit. **(b) For the $q < 1$ regime**, the scalar curvature for the Boltzmann -Gibbs entropy (BG limit) also lies around $T = 0.24$ and is negative but for $q > 1$ the curvature peak becomes positive and is seen to be suppressed for larger q values but they shift towards higher temperatures and here the scalar curvature is zero after the transition takes place in both the the BG limit and $q < 1$ regime.

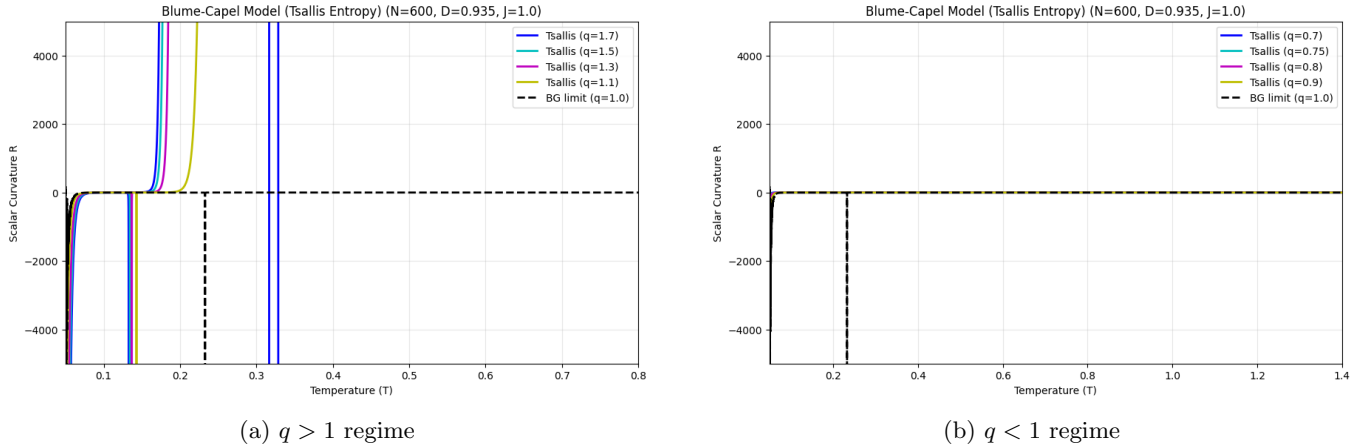


FIG. 3: Temperature dependence of the thermodynamic scalar curvature $R(T)$ for the one-dimensional Blume Capel model using the Tsallis entropy for $(\mathbf{D} < \mathbf{J})$ $D = 0.935$, $J = 1$ and $N = 600$. **(a) For the $q > 1$ regime**, the scalar curvature for the Boltzmann -Gibbs entropy (BG limit) ($q = 1$) lies around $T = 0.24$ and is negative, but for $q > 1$ the curvature peak though still negative shifts towards lower temperatures and the scalar curvature is non zero after the transition takes place for $q > 1$ case whereas it was zero in the previous BG limit. **(b) For the $q < 1$ regime**, the scalar curvature for the Boltzmann -Gibbs entropy (BG limit) also lies around $T = 0.24$ and is negative but for $q > 1$ the curvature peak is completely suppressed for the entire $q < 1$ regime.

V.2. $D > J$: Crystal-Field-Dominated Regime

In the regime $D > J$, the crystal field anisotropy favors the non-magnetic $S = 0$ state, which becomes the dominant configuration, while the magnetic states $S = \pm 1$ are rare. As we see from Fig. 4 and Fig. 5:

In the Boltzmann–Gibbs limit, the scalar curvature again displays a negative peak near $T \approx 0.24$, indicating residual magnetic correlations arising from thermal excitation of the $S = \pm 1$ states. As the temperature increases, the curvature approaches zero, consistent with a paramagnetic regime dominated by uncorrelated fluctuations.

For $q > 1$, the suppression of rare magnetic states further stabilizes the non-magnetic phase. In this case, the curvature peak changes sign and becomes positive, while shifting toward lower temperatures. The positive curvature indicates that the dominant correlations are no longer clustering-type but instead resemble exclusion-driven or repulsive interactions associated with the prevalence of the $S = 0$ state. As observed in the magnetically dominated regime, the scalar curvature remains nonzero beyond the pseudo-transition, highlighting the persistence of correlations generated by the Tsallis deformation.

For $q < 1$, the enhancement of rare magnetic states partially restores magnetic fluctuations. However, these fluctuations do not develop into strong collective behavior. As a result, the curvature peak is significantly suppressed or completely absent, and the scalar curvature remains close to zero over the entire temperature range. This indicates the absence of a dominant correlation structure when rare magnetic states are excessively weighted.

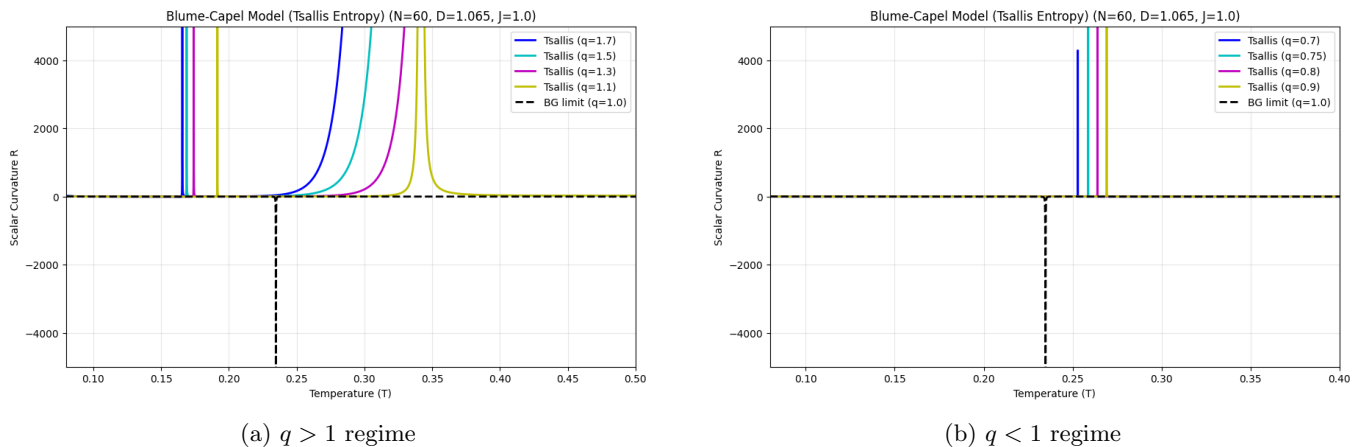


FIG. 4: Temperature dependence of the thermodynamic scalar curvature $R(T)$ for the one-dimensional Blume-Capel model using the Tsallis entropy for $(\mathbf{D} > \mathbf{J})$ $D = 1.065$, $J = 1$ and $N = 60$. **(a) For the $q > 1$ regime**, the scalar curvature for the Boltzmann-Gibbs entropy (BG limit) ($q = 1$) lies around $T = 0.24$ and is negative, but for $q > 1$ the curvature peak becomes positive and shifts towards lower temperatures and the scalar curvature is non zero after the transition takes place for $q > 1$ case whereas it was zero in the previous BG limit. **(b) For the $q < 1$ regime**, the scalar curvature for the Boltzmann-Gibbs entropy (BG limit) also lies around $T = 0.24$ and is negative but for $q > 1$ the curvature peak becomes positive and is seen to be suppressed for larger q values but they shift towards higher temperatures and here the scalar curvature is zero after the transition takes place in both the the BG limit and $q < 1$ regime.

V.3. Finite-Size Effects and Pseudo-Criticality

A comparison between system sizes $N = 60$ and $N = 600$ shows that increasing N has drastic effects particularly for the $q < 1$ regime of the Tsallis modified scalar curvature where the correlation peaks are completely suppressed for $N = 600$ which shows that increasing system size reduces the effects of the rare events considerably whereas for the $q > 1$ regime the correlations survive even after the pseudo transition temperature has been reached. The Tsallis deformation modifies the strength and persistence of correlations in accordance with the size of the system for the spin model.

Overall, the results demonstrate that Tsallis entropy reshapes the geometric structure of the thermodynamic state space by selectively reweighting rare and common microstates. The sign, magnitude, and temperature location of the scalar curvature peak are governed by the interplay between the dominant spin configurations and the nonextensive parameter q . While the Boltzmann–Gibbs limit reflects conventional short-range correlations, deviations from extensivity induce effective long-range correlations that persist beyond the pseudo-transition region. Nevertheless, the absence of curvature divergence reaffirms the pseudo-critical nature of these geometric signatures in the one-dimensional Blume–Capel model.

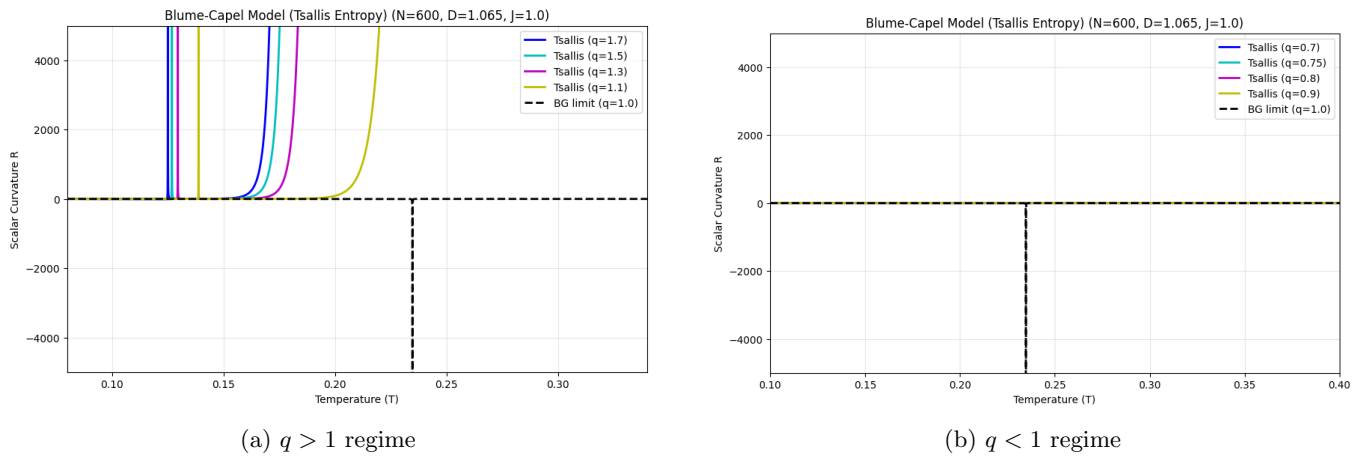


FIG. 5: Temperature dependence of the thermodynamic scalar curvature $R(T)$ for the one-dimensional Blume-Capel model using the Tsallis entropy for $(D > J)$ $D = 1.065$, $J = 1$ and $N = 600$. **(a) For the $q > 1$ regime**, the scalar curvature for the Boltzmann-Gibbs entropy (BG limit) ($q = 1$) lies around $T = 0.24$ and is negative, but for $q > 1$ the curvature peak becomes positive and shifts towards lower temperatures and the scalar curvature is non zero after the transition takes place for $q > 1$ case whereas it was zero in the previous BG limit. **(b) For the $q < 1$ regime**, the scalar curvature for the Boltzmann-Gibbs entropy (BG limit) also lies around $T = 0.24$ and is negative but for $q > 1$ the curvature peak is completely suppressed for the entire $q < 1$ regime.

VI. CONCLUSION

In this work, we have investigated the thermodynamic geometry of the one-dimensional Blume-Capel model within the Tsallis nonextensive statistical framework. By constructing the entropy-based thermodynamic metric as the negative Hessian of the generalized entropy in the parameter space (β, J) , we computed the associated scalar curvature $R(T)$ and analyzed its temperature dependence for both magnetically dominated ($D < J$) and crystal-field dominated ($D > J$) regimes. Although the model does not exhibit a true phase transition at finite temperature, the scalar curvature displays finite peaks that serve as clear geometric signatures of pseudo-critical crossovers. In the Boltzmann-Gibbs limit ($q = 1$), these peaks reflect short-range attractive correlations and vanish smoothly at high temperature, consistent with the absence of genuine criticality in one dimension.

We have shown that the Tsallis deformation parameter q systematically reshapes the entropy surface and modifies the resulting geometric structure. For $q > 1$, the suppression of rare configurations enhances the persistence of correlations and shifts the curvature peak, often maintaining nonvanishing curvature beyond the crossover region. In contrast, for $q < 1$, the enhancement of rare states weakens collective magnetic behavior and can suppress or significantly reduce the curvature peak. Overall, our analysis demonstrates that generalized entropy induces measurable geometric deformations in the thermodynamic manifold, providing a clear information-geometric interpretation of non-extensive effects in low-dimensional spin-1 systems.

VII. ACKNOWLEDGMENTS

The authors would like to thank Bidyut Hazarika and Mozib-Bin-Awal for the help they offered during the course of this work.

-
- [1] F. Weinhold, “Metric geometry of equilibrium thermodynamics,” *J. Chem. Phys.*, vol. 63, pp. 2479–2483, 1975.
 - [2] G. Ruppeiner, “Thermodynamics: A Riemannian geometric model,” *Phys. Rev. A*, vol. 20, no. 4, pp. 1608–1613, 1979.
 - [3] G. Ruppeiner, “Riemannian geometry in thermodynamic fluctuation theory,” *Rev. Mod. Phys.*, vol. 67, no. 3, pp. 605–659, 1995.
 - [4] H. Janyszek, “Riemannian geometry and the thermodynamics of model magnetic systems,” *Reports on Mathematical Physics*, vol. 27, no. 1, pp. 145–159, 1989.

- [5] H. Janyszek and R. Mrugała, “Riemannian geometry and stability of ideal quantum gases,” *Journal of Physics A: Mathematical and General*, vol. 23, no. 4, pp. 467–476, 1990.
- [6] A. Oscoz, E. Mediavilla, M. Serra-Ricart, J. E. Áman, and N. Pidokrajt, “Ruppeiner geometry of black hole thermodynamics,” *European Astronomical Society Publications Series*, vol. 30, pp. 269–273, 2008.
- [7] B. Mirza and M. Zamani-Nasab, “Thermodynamic geometry of a static black hole in $f(R)$ gravity,” *Journal of High Energy Physics*, vol. 2009, no. 06, p. 059, 2009.
- [8] A. Bhattacharjee and P. Phukon, “BTZ Black Hole in the Nonextensive Generalizations of Gibbs Entropy,” *Prog. Theor. Exp. Phys.* **2025**, 023E01 (2025).
- [9] A. Sahay and R. Sanwari, “Thermodynamic geometry of one-dimensional spin one lattice models,” *arXiv preprint arXiv:2011.06491*, 2020.
- [10] R. Sanwari and A. Sahay, “Thermodynamic geometry of spin-one lattice models. I. Spin and quadrupolar orders and critical scaling functions in one dimension,” *Physical Review E*, vol. 105, no. 3, p. 034134, 2022.
- [11] G. Ruppeiner and S. Bellucci, “Thermodynamic curvature for a two-parameter spin model with frustration,” *Physical Review E*, vol. 91, no. 1, p. 012116, 2015.
- [12] M. Blume, “Theory of the first-order magnetic phase change in UO_2 ,” *Phys. Rev.* **141**, 517 (1966).
- [13] H. W. Capel, “On the possibility of first-order phase transitions in Ising systems of triplet ions with zero-field splitting,” *Physica* **32**, 966–988 (1966).
- [14] W. Liu, L. Shi, X. Zhang, X. Li, F. Wang, K. Qi, and Z. Di, “Pseudo transitions in the finite-size Blume-Capel model,” *Phys. Lett. A* **552**, 130626 (2025).
- [15] C. Tsallis, “Possible generalization of Boltzmann–Gibbs statistics,” *Journal of Statistical Physics*, vol. 52, no. 1–2, pp. 479–487, 1988.
- [16] C. Beck and E. G. D. Cohen, “Superstatistics,” *Physica A: Statistical Mechanics and its Applications*, vol. 322, pp. 267–275, 2003.
- [17] M. Gell-Mann and C. Tsallis (eds.), *Nonextensive Entropy: Interdisciplinary Applications*. Oxford University Press, Oxford, 2004.
- [18] S. Abe and Y. Okamoto (eds.), *Nonextensive Statistical Mechanics and Its Applications*. Springer, Berlin, 2001.
- [19] C. Tsallis, *Introduction to Nonextensive Statistical Mechanics: Approaching a Complex World*. Springer, New York, 2009.
- [20] J. Naudts, *Generalised Thermostatistics*. Springer, London, 2011.
- [21] G. B. Bagci and T. Oikonomou, “Deformed entropy and information measures in thermostatistics,” *Physics Letters A*, vol. 373, no. 43, pp. 4341–4345, 2009.
- [22] D. M. Saul, M. Wortis, and D. Stauffer, “Tricritical behavior of the Blume-Capel model,” *Phys. Rev. B* **9**, 4964 (1974).
- [23] T. S. Gunaratnam, D. Krachun, and C. Panagiotis, “Existence of a tricritical point for the Blume–Capel model on \mathbb{Z}^d ,” *Probab. Math. Phys.* **5**, 785–845 (2024).
- [24] W. Kwak, J. Jeong, J. Lee, and D.-H. Kim, “First-order phase transition and tricritical scaling behavior of the Blume-Capel model: A Wang-Landau sampling approach,” *Phys. Rev. E* **92**, 022134 (2015).
- [25] A. M. Goldman, “Tricritical points of thin superconducting films,” *Phys. Rev. Lett.* **30**, 1038 (1973).
- [26] L. Moueddene, N. G. Fytas, Y. Holovatch, R. Kenna, and B. Berche, “Critical and tricritical singularities from small-scale Monte Carlo simulations: the Blume–Capel model in two dimensions,” *J. Stat. Mech.: Theory Exp.* **2024**, 023206 (2024).
- [27] M. Azhari and U. Yu, “Tricritical point in the mixed-spin Blume-Capel model on three-dimensional lattices: Metropolis and Wang-Landau sampling approaches,” *Phys. Rev. E* **102**, 042113 (2020).
- [28] H. W. J. Blöte and Y. Deng, “Revisiting the field-driven edge transition of the tricritical two-dimensional Blume-Capel model,” *Phys. Rev. E* **99**, 062133 (2019).
- [29] I. Mandal, S. Inglis, and R. G. Melko, “Geometrical mutual information at the tricritical point of the two-dimensional Blume–Capel model,” *J. Stat. Mech.: Theory Exp.* **2016**, 073105 (2016).
- [30] F. Antenucci, A. Crisanti, and L. Leuzzi, “Critical study of hierarchical lattice renormalization group in magnetic ordered and quenched disordered systems: Ising and Blume–Emery–Griffiths models,” *J. Stat. Phys.* **155**, 909–931 (2014).
- [31] G. D. Mahan and S. M. Girvin, “Blume-Capel model for plane-triangular and fcc lattices,” *Phys. Rev. B* **17**, 4411 (1978).
- [32] M. Clusel, J.-Y. Fortin, and V. N. Plechko, “Alternative description of the 2D Blume–Capel model using Grassmann algebra,” *J. Phys. A: Math. Theor.* **41**, 405004 (2008).
- [33] C. J. da Silva, A. A. Caparica, and J. A. Plascak, “Wang-Landau Monte Carlo simulation of the Blume-Capel model,” *Phys. Rev. E* **73**, 036702 (2006).
- [34] D. A. Dias and J. A. Plascak, “Site-diluted Blume–Capel model for the Fe–Al disordered alloys,” *Phys. Lett. A* **375**, 2089–2093 (2011).
- [35] D. Peña Lara, G. A. Pérez Alcázar, L. E. Zamora, and J. A. Plascak, “Blume-Capel model for $(\text{Fe}_{0.65}\text{Ni}_{0.35})_{1-x}\text{Mn}_x$ and $\text{Fe}_p\text{Al}_q\text{Mn}_x$ alloys,” *Phys. Rev. B* **80**, 014427 (2009).
- [36] A. Blatter and M. Von Allmen, “Reversible amorphization in laser-quenched titanium alloys,” *Phys. Rev. Lett.* **54**, 2103 (1985).
- [37] W. Sinkler *et al.*, “Neutron-diffraction investigation of structural changes during inverse melting of $\text{Ti}_{45}\text{Cr}_{55}$,” *Phys. Rev. B* **55**, 2874 (1997).
- [38] K. I. Mazzitello, J. Candia, and E. V. Albano, “Far-from-equilibrium growth of magnetic thin films with Blume-Capel impurities,” *Phys. Rev. E* **91**, 042118 (2015).
- [39] M. Kaufman, S. Kaufman, and H. T. Diep, “Social depolarization: Blume–Capel model,” *Physics* **6**, 138–147 (2024).
- [40] H. T. Diep, M. Kaufman, and S. Kaufman, “Monte Carlo study of agent-based Blume-Capel model for political depolarization,” in *EPJ Web of Conferences*, Vol. **300**, 01005 (2024).

- [41] V. Mozolenko and L. Shchur, “Blume-Capel model analysis with a microcanonical population annealing method,” *Phys. Rev. E* **109**, 045306 (2024).
- [42] E. N. M. Cirillo, V. Jacquier, and C. Spitoni, “Homogeneous and heterogeneous nucleation in the three-state Blume–Capel model,” *Physica D* **461**, 134125 (2024).
- [43] H. Akın, “Investigation of thermodynamic properties of mixed-spin (2, 1/2) Ising and Blume–Capel models on a Cayley tree,” *Chaos Solitons Fractals* **184**, 114980 (2024).
- [44] A. S. Ovchinnikov *et al.*, “Influence of the type of intercalation on spin-glass formation in the Fe-doped TaS₂(Se₂) polytype family,” *Phys. Rev. B* **109**, 054403 (2024).
- [45] H. Janyszek and R. Mrugała, “Riemannian geometry and stability of thermodynamical equilibrium systems,” *Physical Review A*, vol. 39, no. 12, pp. 6515–6523, 1989.
- [46] G. Ruppeiner, “Thermodynamic curvature measures interactions,” *American Journal of Physics*, vol. 78, no. 11, pp. 1170–1180, 2010.
- [47] J. E. Aman, I. Bengtsson, and N. Pidokrajt, “Geometry of black hole thermodynamics,” *General Relativity and Gravitation*, vol. 35, no. 10, pp. 1733–1743, 2003.
- [48] B. Mirza and M. Zamani-Nasab, “Ruppeiner geometry of RN black holes: Flat or curved?,” *Journal of High Energy Physics*, vol. 2007, no. 06, p. 059, 2007.
- [49] S. Amari, *Differential-Geometrical Methods in Statistics*. Springer, 1985.
- [50] G. E. Crooks, “Measuring thermodynamic length,” *Physical Review Letters*, vol. 99, no. 10, p. 100602, 2007.